Supplemental Data

PINK1 deficiency impairs mitochondrial homeostasis promoting lung fibrosis

Marta Bueno[1,2], Yen-Chun Lai[1], Yair Romero[3], Judith Brands[1,2], Claudette StCroix[4], Christelle Kamga[1], Catherine Corey[1], Jose D. Herazo-Maya[5], John Sembrat[1,2,], Janet S. Lee[2], Steve R. Duncan[2], Mauricio Rojas[2,6], Sruti Shiva[1,7], Charleen T. Chu[8], and Ana L Mora[1,2 *]

Table S1. Demographics characteristics of patient cohort.

	Donor-Control Young	Donor -Control Old	IPF
Subjects	12	7	22
Age	28-48	50-72	55-78
Gender			
Female	6 (50%)	3 (43%)	9 (41%)
Male	6 (50%)	4 (57%)	13 (59%)

Table S2. Demographics and clinical characteristics of the LGRC cohort.

Phenotype	**Control**	**IPF**
Subjects (n)	96	123
Age		
Mean	63.88 ± 11.24	64.78 ± 8.27
Range	34 - 87	40 - 82
Gender		
Male	46 (47.9 %)	82 (66.7 %)
Female	50 (52.1 %)	41 (33.3 %)
Race		
White (Caucasian)	88 (91.6 %)	113 (91.8 %)
Hispanic	2 (2.08 %)	1 (0.81 %)
African American	3 (3.125 %)	5 (4.06 %)
Native American	1 (1.04 %)	0
Asian/Pac islander	1 (1.04 %)	2 (1.62 %)
Other	1 (1.04 %)	2 (1.62 %)
PFTs		
FEV1%	95 ± 13.31	71.44 ± 17.62
FVC%	94.78 ± 13.33	64.56 ± 16.42
DLCO%	82.75 ± 17	48.77 ± 18
Smoking (ppy)	34.7 ± 29.9	25.1 ± 21

Table S3. Significant gene sets correlated with PINK1 expression*		
Standard gene-set name	**Gene-set description**	**Max mean score**
BIOCARTA_TALL1_PATHWAY	TACI and BCMA stimulation of B cell immune responses	-1.11
BIOCARTA_CASPASE_PATHWAY	Caspase Cascade in Apoptosis	-0.93
BIOCARTA_MITOCHONDRIA_PATHWAY	Role of Mitochondria in Apoptotic Signaling	-0.92
BIOCARTA_BARRESTIN_SRC_PATHWAY	Roles of fl-arrestin-dependent Recruitment of Src Kinases in GPCR Signaling	0.81
BIOCARTA_PTEN_PATHWAY	PTEN dependent cell cycle arrest and apoptosis	0.77
BIOCARTA_DEATH_PATHWAY	Induction of apoptosis through DR3 and DR4/5 Death Receptors	-0.76
BIOCARTA_MYOSIN_PATHWAY	PKC-catalyzed phosphorylation of inhibitory phosphoprotein of myosin phosphatase	0.68
BIOCARTA_AKAPCENTROSOME_PATHWAY	Protein Kinase A at the Centrosome	0.63
BIOCARTA_IGF1R_PATHWAY	Multiple antiapoptotic pathways from IGF-1R signaling lead to BAD phosphorylation	0.62
BIOCARTA_FAS_PATHWAY	FAS signaling pathway (CD95)	-0.54
BIOCARTA_PTDINS_PATHWAY	Phosphoinositides and their downstream targets	0.52
BIOCARTA_HIVNEF_PATHWAY	HIV-I Nef: negative effector of Fas and TNF	-0.48

*A positive gene-set is one in which higher expression of most genes in the gene set correlate with higher PINK1 expression. A negative gene-set is one in which lower expression of most genes in the gene set correlate with higher PINK1 expression. The gene set order in the table is determined by the Maxmean score, whichever larger in absolute values. Statistical significance was defines as FDR<5%.

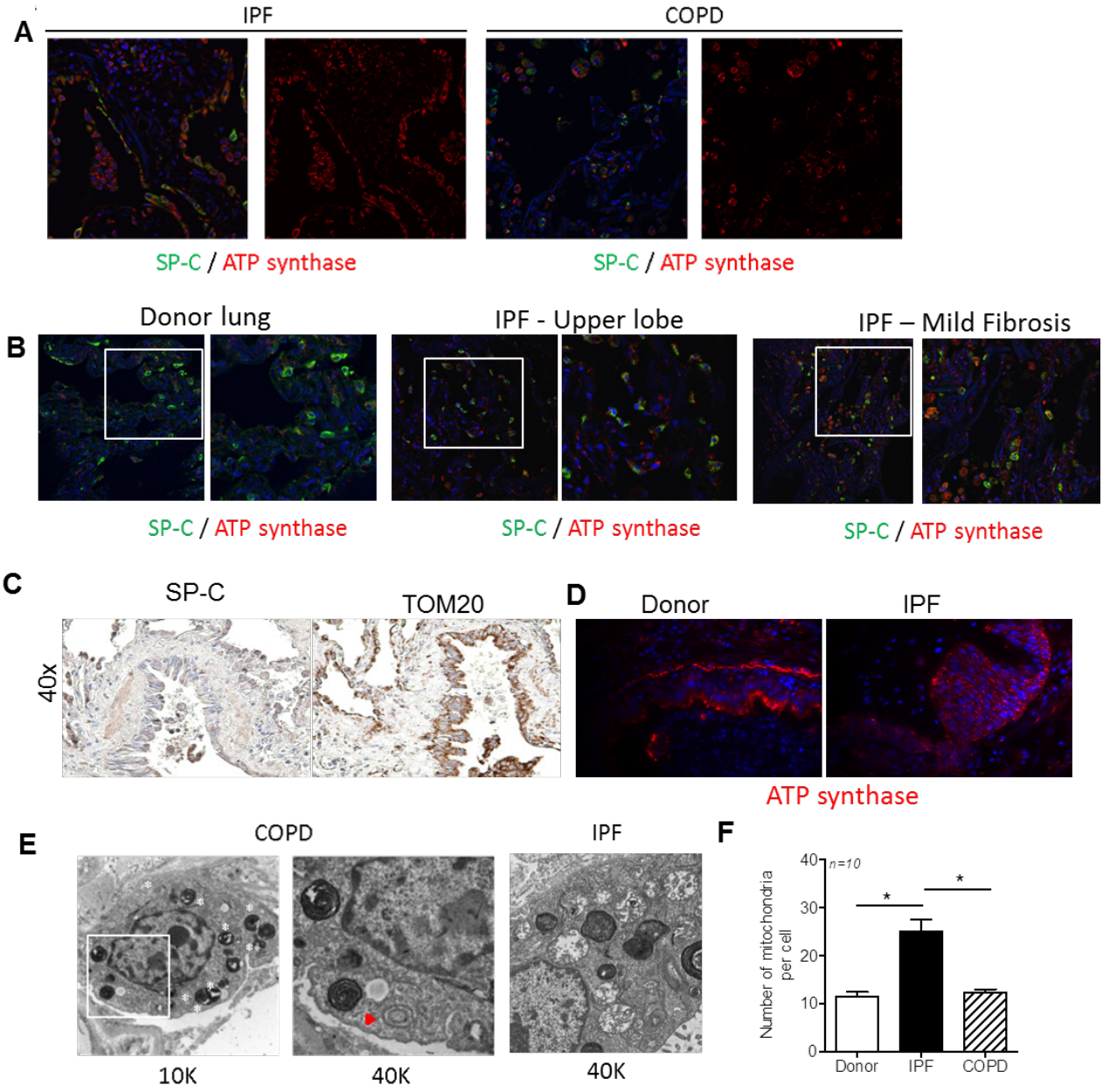

Supplemental Figure 1. Accumulation of mitochondria in hyperplasic AECII located in honeycombs from IPF lungs (A) Merged low magnification image (20x) from immunofluorescence analyses using anti-SP-C (green, AECII marker) and anti-ATP synthase I (red, mitochondrial marker) antibodies in IPF and COPD lungs showing accumulation of

mitochondria only in hyperplasic AECII from honeycombs in IPF lung. Right panels: red channel (mitochondria marker only). **(B)** Representative images of analyses using anti-SP-C (green, AECII marker) and anti-ATP synthase I (red, mitochondrial marker) antibodies in donor control lung and IPF lungs in areas from upper lobe and mild fibrosis (40x magnification). Inset boxes are shown at higher magnification. Notice co-localization of epithelial and mitochondria markers in IPF lungs is at similar levels than donor control lung. **(C)** Representative image of immunohistochemistry analyses in consecutive sections of IPF lung using SP-C and Tom20 antibody showing airway section (40x magnification). Notice high positivity for mitochondrial marker in airway epithelial cells. (**D**) Immunofluroescence for ATP synthase (mitochondrial marker) of airway epithelial cells in donor control and IPF lung (n=5 per condition, 40x magnification). **(E)** Representative TEM images of AECII from COPD lungs identified by the presence of lamellar bodies. Red arrow: double membrane autophagosome. **(F)** Determination of number of mitochondria per cell in TEM COPD images confirmed mitochondrial numbers similar to the donor lungs (n=10 per condition). Data represent the mean ± SEM **(F)**. *$p<0.01$ by one-way ANOVA with post hoc Bonferroni **(F)**.

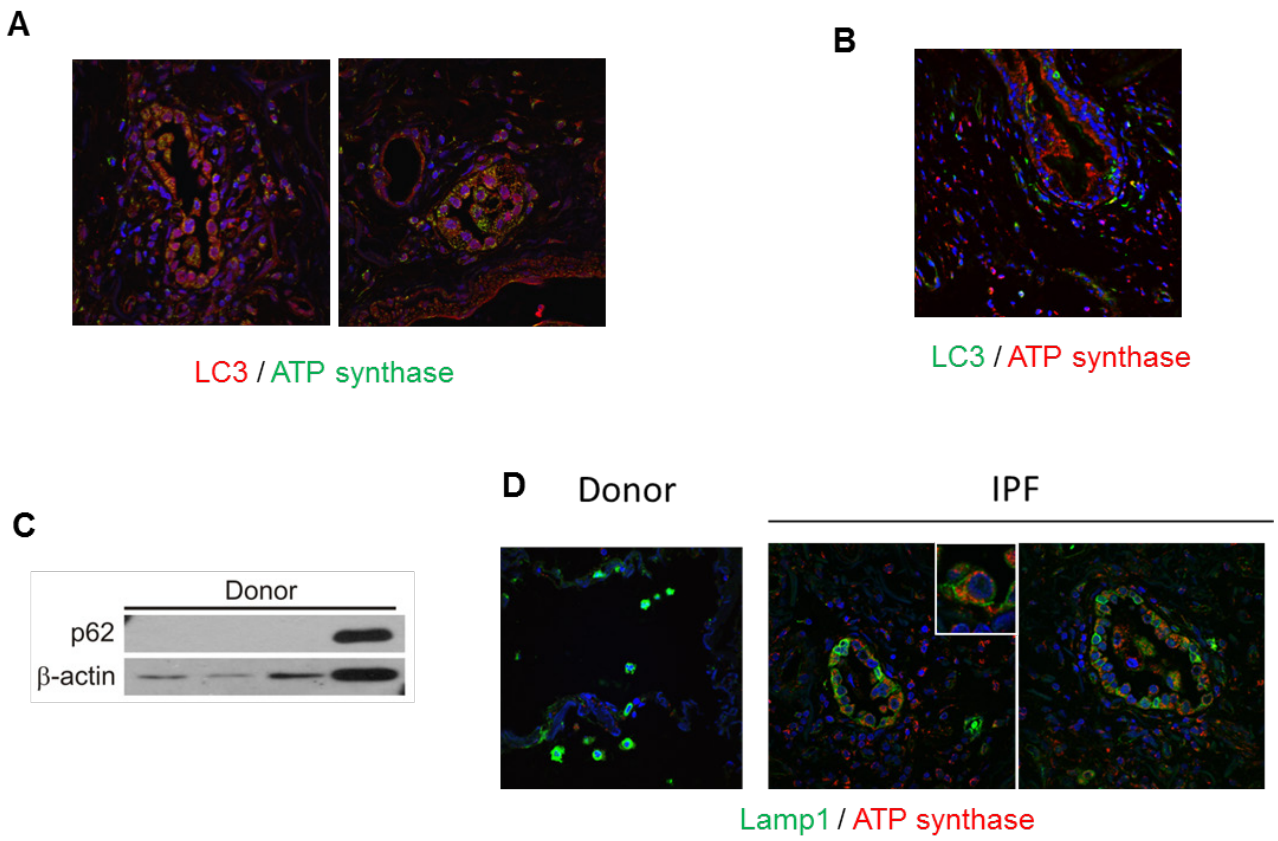

Supplemental Figure 2. Late blockade of autophagy flux in AECII from IPF lungs (A) Representative images of immunofluorescence analyses in IPF lungs using anti-LC3 (red staining) and anti-ATP synthase (green staining) antibodies. Notice positive staining of LC3 in epithelial cells localized in honeycombs. (20x magnification). **(B)** Representative images of immunofluorescence analyses in IPF lungs using anti-LC3 (green staining) and anti-ATP synthase (red staining) antibodies showing airway epithelial cells are positive for ATP synthase (mitochondria marker) but negative for LC3. (20x magnification). **(C)** Western blot analyses in isolated AECII from donor control lungs using anti-p62 antibody. Blot was stripped and reblotted with anti-βactin antibody for determination of loading control (derived from the same experiment as Supplemental Figure 5A). **(D)** Representative images of immunofluorescence

analyses in donor control and IPF lungs using anti-Lamp1 (green staining, lysosomal marker), and ATP synthase (red staining, mitochondria marker). Notice low levels of Lamp1 in cells highly positive for ATP synthase. (20x magnification).

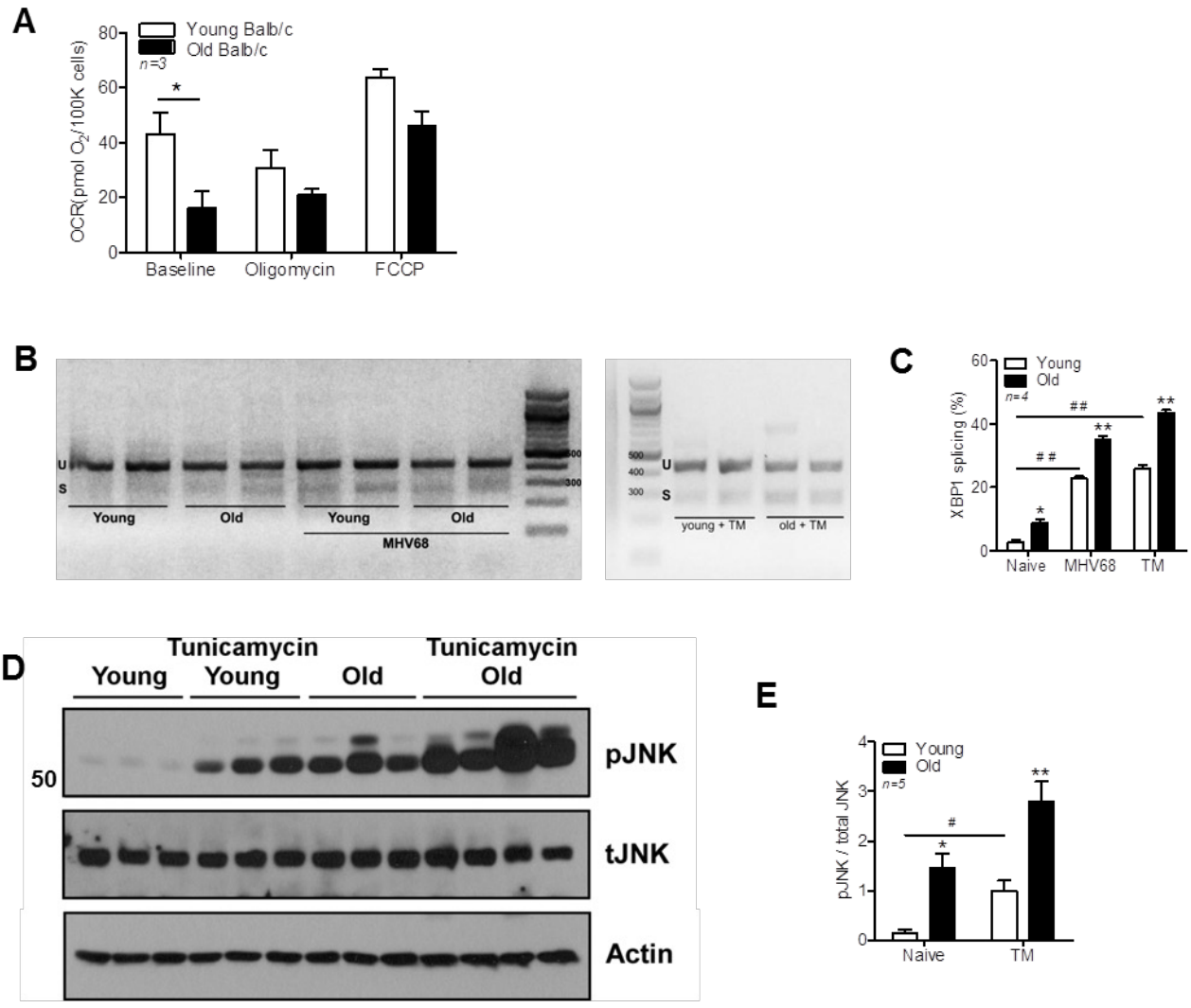

Supplemental Figure 3. ER stress impairs mitochondrial respiration (A) Mitochondria respiration parameters in isolated primary AECII from young and aging Balb/c mice. Mitochondria from aging mice showed significant decreased in basal respiration, and maximal mitochondrial respiration measured by treatment with FCCP (n=3 per condition). **(B)** Representative images of splicing of XBP1 after intra-tracheal instillation of TM (2μg per mouse) and MHV68 infection in young and old mice. Each lane represents an individual mouse. **(C)** Quantification of XBP1 splicing in young and old mice. **(D)** Phosphorylation levels of JNK

in lungs from young and old mice treated with vehicle control and TM. Blot was stripped and re-blotted with anti-JNK and β-actin antibodies for determination of total JNK protein and loading control. **(E)** Densitometry analyses for determination of p-JNK levels in young and old mice with vehicle control or TM treatment. Old mice presented JNK activation even before TM treatment. Data represent mean ± SEM (**A**, **C** and **E**). *p<0.05 and **p<0.01 vs. young (**A, C** and **E**), #p<0.05 and ##p<0.01 (**C** and **E**) by unpaired 2-tailed Student's *t* test (**A**) and two-way ANOVA with post hoc Bonferroni (**C** and **E**).

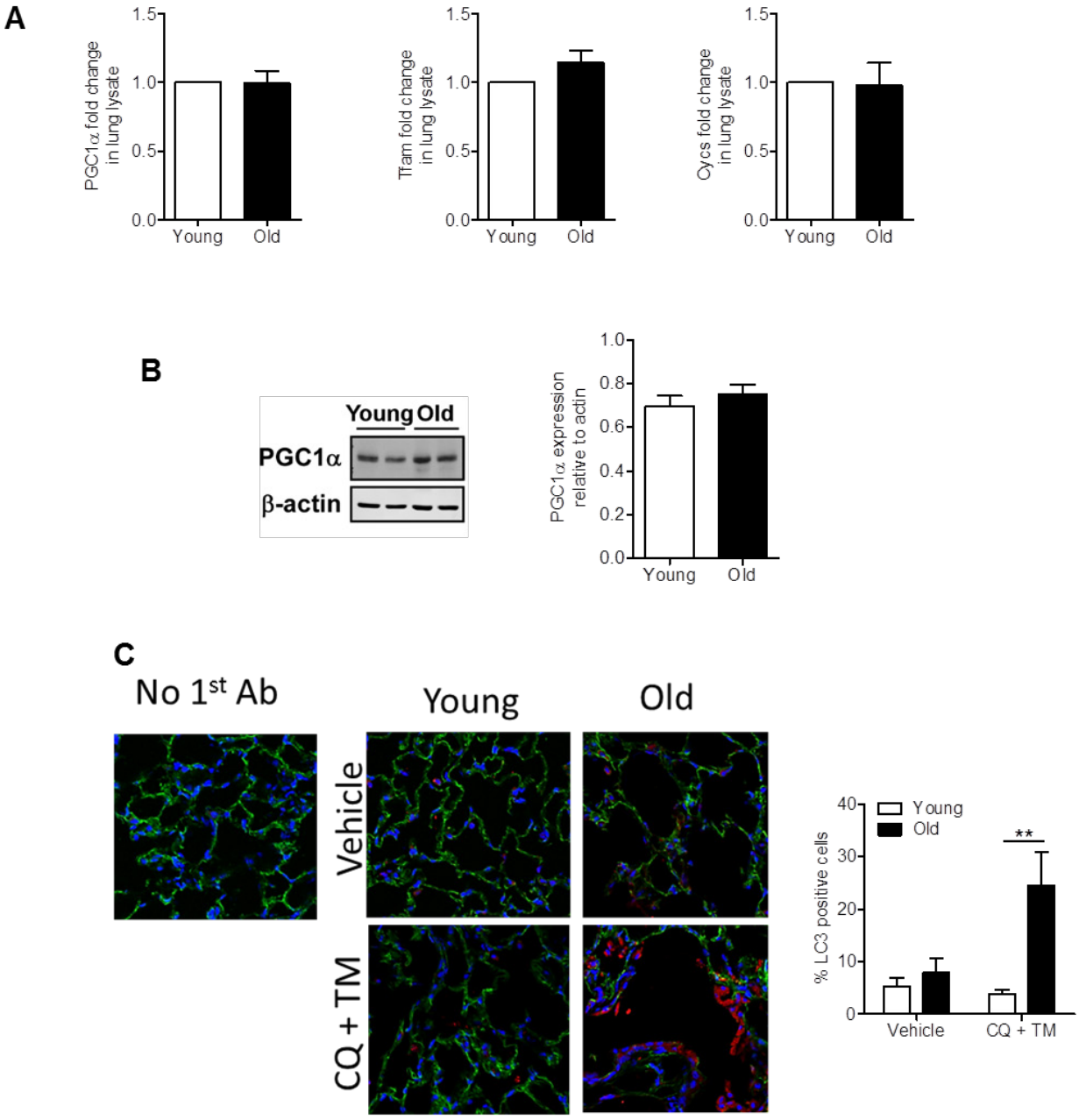

Supplemental Figure 4. **Young and old mice show comparable mitochondria biogenesis but different mitophagy flux. (A)** qPCR analysis of mitochondrial biogenesis markers. PGC1α, Tfam and Cysc show no significant change in the biogenesis between young and old mice. **(B)** Representative western bot analysis of PGC1α confirms that there are no changes in the

biogenesis with age (quantification on the right side). **(C)** Representative images of lungs of young and old mice treated intratracheally with TM (20 μg per mouse) and chloroquine (2 mg /Kg weight) and analyzed 4 h later for LC3 levels (red staining). DAPI staining was used for nuclear counterstaining and anti-β-actin (green) staining for visualization of lung structure. Control staining was performed without incubation with anti-LC3 antibody. Semi-quantitative analyses of percentage of LC3 positive cells showed increased LC3 staining in lungs from old mice treated with TM and chloroquine. Data represent mean ± SEM (**A**-**C**). **$p<0.01$ by unpaired 2-tailed Student's *t* test (**A** and **B**) and two-way ANOVA with post hoc Bonferroni (**C**).

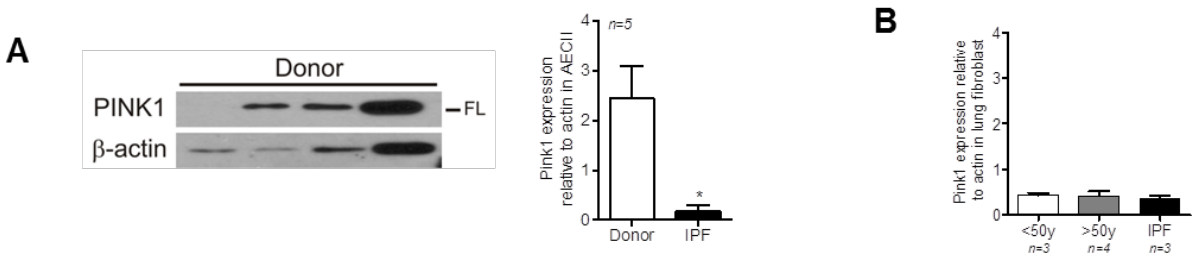

Supplemental Figure 5. PINK1 expression in different primary cell types (A) Western blot analyses of whole lysates of isolated AECII from donor control lungs using anti-PINK1 antibody (FL, full length). Each lane represents an individual patient. Quantification at the right show significant diminution of PINK1 levels in AECII from IPF lungs (n=5 per condition). Anti-βactin was derived from the same experiment as Supplemental Figure 2C. **(B)** Quantification of western blot analyses of PINK1 expression in isolated lung fibroblasts from donor control and IPF patients (representative image in Figure 7F). Donor controls were subdivided in young (<50 years old) and old (>50 years old) individuals. Similar expression levels of PINK1 were found in fibroblasts from donor and IPF patients. Data represent mean ± SEM (**A**-**B**). *p<0.05 by unpaired 2-tailed Student's *t* test (**A**) and one-way ANOVA with post hoc Bonferroni (**B**).

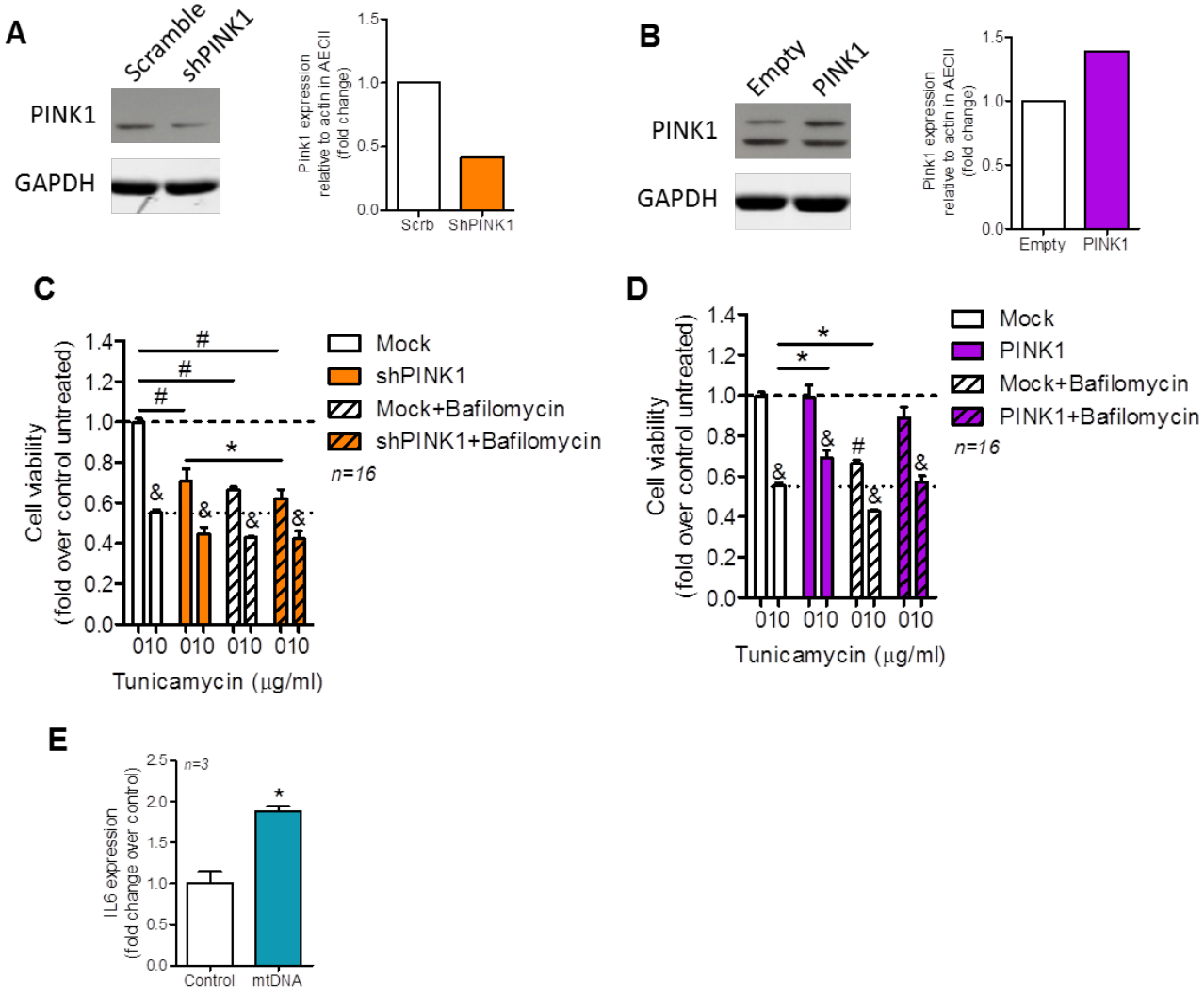

Supplemental Figure 6. In vitro knockdown and upregulation of PINK1 have an effect in A549 cell survival (A) PINK1 was down-modulated in A549 by transfection with shPINK1 (Scramble as control). **(B)** A549 cells were transfected with empty vector or PINK1 cDNA to overexpress the protein. **(C)** Cell viability data from treatments showed in Figure 8A. A549 cells transfected with PINK1-shRNA showed reduction of cell viability after tunicamycin (10µg/ml) and bafilomycin A1 treatments (10nM). **(D)** Cell viability data from treatments showed in Figure

8B. Cell survival is improved with PINK1 overexpression in A549 cells even in the presence of tunicamycin (10μg/ml) and/or bafilomycin A1 (10nM). **(E)** IL6 mRNA levels increase after mtDNA treatment in A549 cells (n=3 per condition). Data represent mean ± SEM (**C**-**E**). $^{\&}p<0.05$ vs. TM untreated for each condition (**C** and **D**), #p<0.05 vs. mock TM untreated (**C** and **D**), *p<0.05 as is indicated (**C**-**E**) by one-way ANOVA with post hoc Bonferroni (**C**-**D**) and unpaired 2-tailed Student's *t* test (**E**).

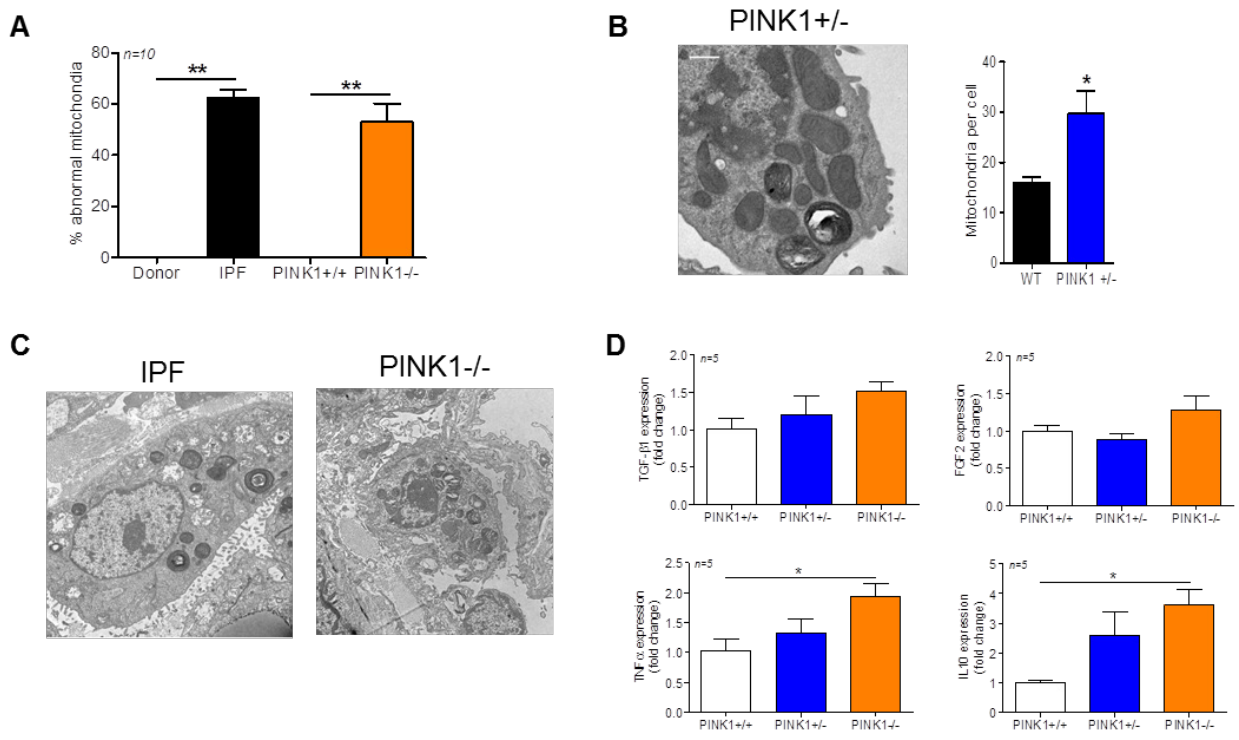

Supplemental Figure 7. Characterization of the lungs of untreated PINK1 deficient mice. (A) Percentage of AECII abnormal mitochondria (swollen with evidence of severely disrupted cristae over all mitochondria) from TEM images of donor and IPF patients, and PINK1 deficient mice. **(B)** Representative TEM image of 9 months old PINK1 +/- deficient mice showing accumulation of swollen mitochondria in AECII. Notice large mitochondria profiles with low number of crista. Morphometric analyses of TEM images showed increased number of mitochondria per AECII in PINK1+/- mice in comparison to wild type age-matched controls (n=10 cells per condition). **(C)** Representative images (10K magnification) of IPF lung and naïve PINK1-/- mouse showing similarities in their mitochondrial profiles and percentages of abnormal mitochondria. Regions of collagen fibrils inside the alveolar walls and surrounding type II epithelial cells are present in both samples. **(D)** Relative change in the levels of TGF-β,

FGF2, TNFα and IL10 transcripts in lung of naïve wild type (white bar) and PINK1+/- (blue) and -/- (orange) deficient mice. Data represent mean ± SEM (**A**-**B** and **D**). *p<0.05 and **p<0.01 by unpaired 2-tailed Student's *t* test (**A**-**B**) and one-way ANOVA with post hoc Bonferroni (**D**).

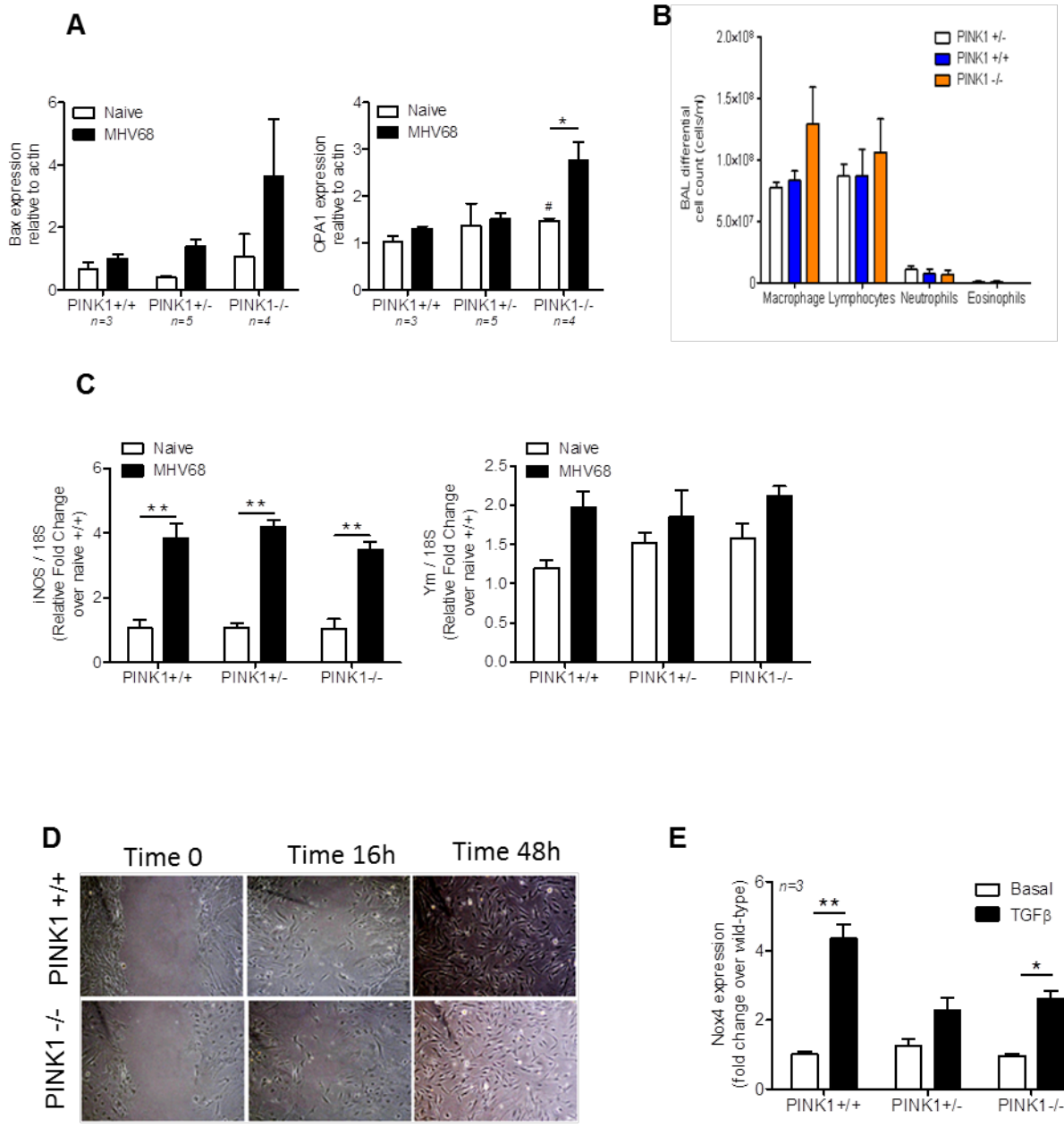

Supplemental Figure 8. Characterization of the lungs of MHV68 infected PINK1 deficient mice (A) Quantification of western blot analyses of whole lung lysates from naïve and MHV68 infected PINK1+/+, +/- and -/- mice using anti-Bax and anti-OPA1 antibodies. **(B)** Bronchalveolar lavage cell counts after MHV68 infection were not statistically significant

between PINK1 +/+ (white bars), +/- (blue bars), and -/- (orange bars) (n=3-5 per group). **(C)** Expression of Th1 and Th2 macrophage markers in total lung lysate of naïve and MHV68 infected PINK1 deficient mice. **(D)** Representative images of wound closing assays with isolated lung fibroblasts from PINK1 +/+ and -/- mice. No significant differences were observed between wild type and PINK1 deficient mice. **(E)** Relative change in the levels of Nox4 transcripts in lung fibroblasts isolated from wild type and PINK1 deficient mice before and after TGF-β stimulation (2 ng/ml for24 h) Data represent mean ± SEM (**A**-**C** and **E**). #$p<0.05$ vs. PINK1 +/+ naïve (**A**); *$p<0.05$ and **$p<0.01$ as indicated (**A**, **C** and **E**) by two-way ANOVA with post hoc Bonferroni (**A**, **C** and **E**) and one-way ANOVA with post hoc Bonferroni (**B**).

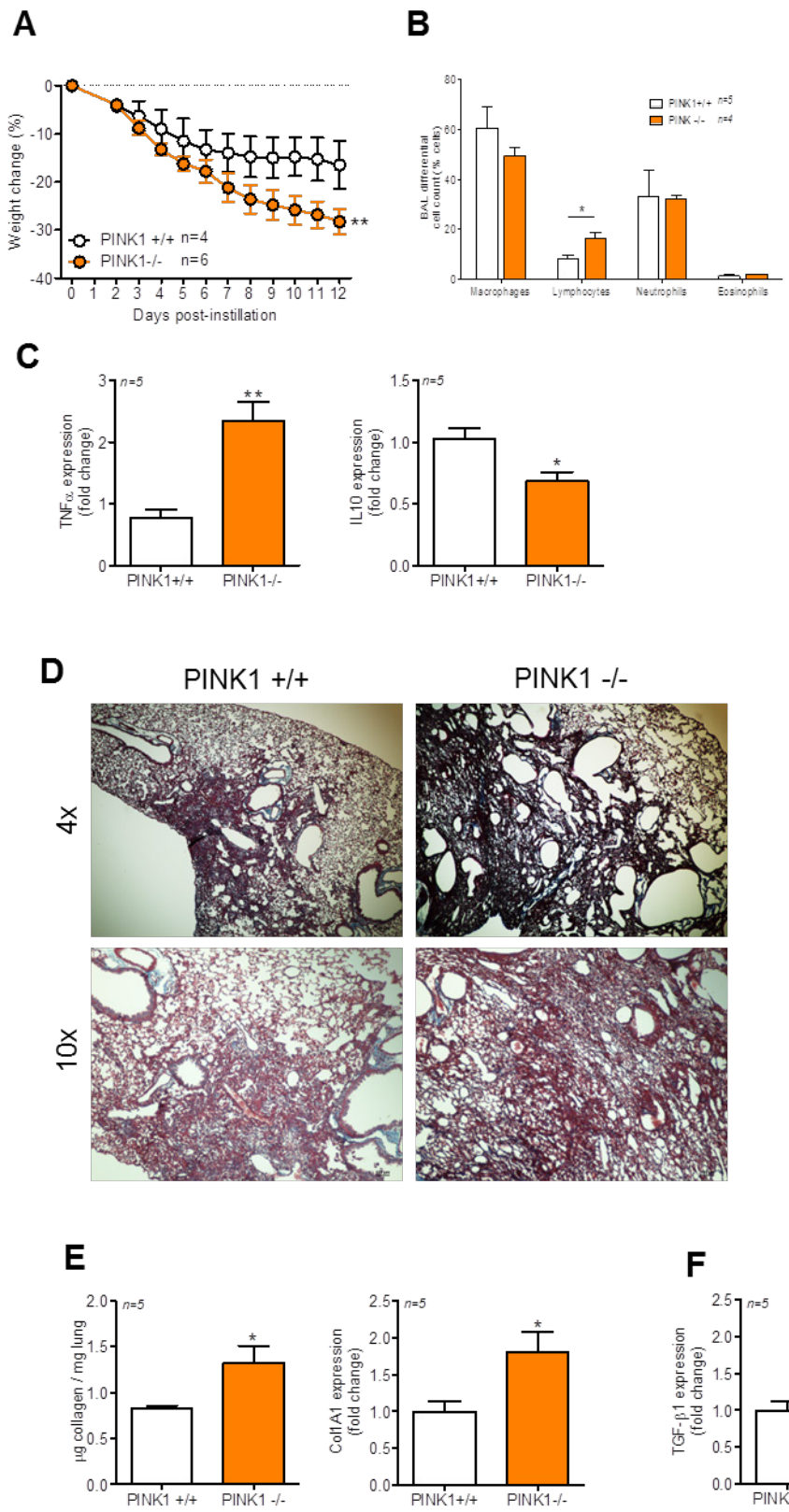
A
Weight change (%)
0
-10
-20
-30
-40
PINK1 +/+ n=4
PINK1-/- n=6
**
0 1 2 3 4 5 6 7 8 9 10 11 12
Days post-instillation
B
BAL differential cell count (% cells)
80
60
40
20
0
PINK1+/+ n=5
PINK -/- n=4
*
Macrophages
Lymphocytes
Neutrophils
Eosinophils
C
TNFα expression (fold change)
n=5
**
PINK1+/+
PINK1-/-
IL10 expression (fold change)
n=5
*
PINK1+/+
PINK1-/-
D
PINK1 +/+
PINK1 -/-
4x
10x
E
µg collagen / mg lung
n=5
*
PINK1 +/+
PINK1 -/-
Col1A1 expression (fold change)
n=5
*
PINK1+/+
PINK1-/-
F
TGF-β1 expression (fold change)
n=5
*
PINK1+/+
PINK1-/-

Supplemental Figure 9. PINK1 deficient mice are more susceptible to bleomycin induced lung fibrosis. Young mice (3 months old) were treated with a bleomycin dose of 2U/kg (administered intra-tracheally) and sacrificed for organ harvest at day 15 post-instillation. **(A)** Weight loss data in wild type and deficient PINK1 mice after bleomycin treatment. **(B)** Bronchalveolar lavage cell counts at day 15 after bleomycin (*$p<0.05$ vs. PINK1+/+). **(C)** Relative change of TNF-α and IL10 transcripts in lung after bleomycin injection in wild type and PINK1 deficient mice. **(D)** Representative Masson trichrome staining in lung sections from PINK1 +/+ and -/- showing increased collagen deposition (blue) at day 15 post-bleomycin. **(E)** Increased collagen deposition in lungs of PINK1 deficient mice after bleomycin treatement determined by OH-proline levels and RNA expression levels of collagen I. **(F)** Relative change of TGF-β transcripts in lung after bleomycin instillation in wild type and PINK1 deficient mice. Data represent mean ± SEM (**A**-**C** and **E**-**F**). *$p<0.05$ and **$p<0.01$ by one-way repeated measures ANOVA with post hoc Bonferroni (**A**) and unpaired 2-tailed Student's t test (**B**-**C** and **E**-**F**).